Effect of Nitriding Temperature on the Nanostructure and Corrosion Properties of Nickel Coated 304 Stainless Steel

A. R. Grayeli Korpi[1] and Kh. M. Bahmanpour[2]

[1.] Physics and Accelerators Research School, Nuclear Sciences and Technology Research Institute, P. O. Box: 11365-3486, Tehran,Iran.

[2.] Plasma Physics Research Center, Science & Research Branch, Islamic Azad University, P. O. Box: 14665-678, Tehran, Iran

ABSTRACT

Nickel films of 150 nm thickness were deposited on 304 stainless steel and post annealed under flow of nitrogen at different temperatures. The prepared samples were corrosion tested in 1.0 M H_2SO_4 solution using potentiodynamic polarization technique. Crystallographic and morphological structure of the samples were analyzed by X-ray diffraction (XRD) and atomic force microscopy (AFM), respectively, before corrosion test, and scanning electron microscope (SEM) after corrosion test. A clear correlation between the physical analyses (XRD, AFM and SEM) and the potentiodynamic results is achieved. The variation of corrosion resistance of the samples showed that the optimum annealing temperature is 673 K. Prog. Color Colorants Coat. 10 (2017), 85-92© Institute for Color Science and Technology.

1. Introduction

In addition to desirable physical and mechanical properties of stainless steels, the most important property of these alloys, which determines their use, is their ability to withstand corrosion in various environments. During the past decades, multifarious methods of surface modification techniques such as physical vapor deposition, annealing, gas nitriding, ion nitriding, and ion implantation have been conducted to improve corrosion behavior of austenitic stainless steels [1– 9].

The properties of a specific steel type will thus be determined by the combined effect of the alloying and trace elements in that specific grade. Therefore, by changing the amount of each element in the alloy composition, it is possible to obtain different corrosion behavior. Although the corrosion resistance of stainless steels comes from the presence of chromium, the highest resistance to uniform corrosion is obtained with the nickel-bearing asthenic types, and, in general, the highest nickel-composition alloys in this class are more resistant than the lowest nickel composition [9–14].

Nickel alloys are widely used in chemical process, petrochemical, pulp and paper, energy conversion, power production, supercritical water, waste incineration, pharmaceutical, and many other industries where a better corrosion resistance is required, and the main reason for adding nickel is to promote an austenitic structure. On the other hand, nitrogen as a remarkable austenitic former normally present in commercial alloys to the extent of a few hundredths percent. Although nitrogen forms chromium nitrides, it is less effective than carbon in causing damage,

perhaps in part because nitrides precipitate more generally throughout the grains or they form islands along grain boundaries, interrupting a continuous path along which the corrosive agent can proceed [14].

Although much less literature has been published about nickel nitrides due to the difficulties to synthesize its nitrides, nickel nitrides can be obtained by a few methods such as nitriding in gaseous ammonia, reactive sputtering or ion beam implantation [15-19]. We also reported the surface properties of stainless steel by introducing nitrogen ion implantation following to the deposition of nickel in previous studies [1].

Therefore, due to above mentioned properties and applications of both nitrogen and nickel and in order to enhance the corrosion resistance of stainless steel, it is worthwhile to mention that this work presents a new method for protection of 304 stainless steel in H_2SO_4 solution using PVD deposition of Ni and thermal treatment of N_2 in form of nickel nitride thin films. Also, there is a good correlation between our XRD, AFM, SEM, and potentiodynamic polarization analyses which confirms the proposed idea.

2. Experimental

Nickel films of 150 nm thickness were deposited on 304 stainless steels (18 mm × 18 mm × 1 mm) by electron beam evaporation (PVD-EB, E19A3 Edwards model, England) at room temperature. The purity of nickel was 99.98%. A base pressure of 2×10^{-7} mbar was used. The deposition rate was measured by a quartz crystal deposition rate controller (Sigma Instruments, SQM- 160, USA) positioned close to the substrate.

Prior to deposition, all substrates were ultrasonically cleaned in heated acetone and then ethanol. Post-annealing of the Ni films was performed at four different temperatures of 523, 673, 823, 973 K in nitrogen environment with a flow rate of 600 cm^3min^{-1}. The atmosphere air of the annealing tube was flushed with argon gas several times before introducing nitrogen and heating the samples.

Crystallographic structure of these films was obtained using a STOE model STADI MP Diffractometer, Germany (CuKα radiation) with a step size of 0.01° and count time of 1.0 s per step, while the surface physical morphology/nanostructure and roughness was obtained by means of AFM analysis (Auto Probe Pc, Park Scientific Instrument, USA; in

contact mode, with low stress silicon nitride tip of less than 200 A° radius and tip opening of 18°) and scanning electron microscope (SEM: LEO 440i, England).

Electrochemical behavior of the samples was achieved using potentiodynamic method with a potentiostat coupled to PC (273A, EG& G, USA). In order to carry out this analysis, an area of 1.0 ± 0.05 cm^2 was exposed to the acidic environment. The samples were polarized in 1.0 M H_2SO_4, a solution made of analytical grade reagent and double distilled water.

3. Results and discussion

3.1. XRD results

Figure 1 shows the XRD patterns of the post-annealed Ni/SS films at four different temperatures using nitrogen flow and 304 SS substrates. XRD pattern of untreated sample mostly shows the presence of austenite peaks at 2θ = 43.7°, 50.7°, 74.8° and 90.0° that correspond to γ–Fe(111), γ–Fe(200), γ–Fe(220) and γ–Fe(311), respectively. In addition to the original stainless steel peaks, the diffraction peaks in the annealed samples mainly show nickel nitride diffraction lines.

The effect of annealing temperature with flow of nitrogen on different samples can be observed as emergence of nickel nitride phases in XRD patterns. Examination of the XRD patterns of sample prepared at 523K annealing temperature with the flow of nitrogen showed one peak which can be designated to $Ni_3N(111)$ at 2θ = 44.485°. For the higher annealing temperatures of 673 and 823 K, the peak of $Ni_3N(111)$ has intensified. The great intensity of nickel nitride peak at 673 and 823 K indicates that at these temperatures, highest amount of nitride is formed.

There is a phase transition in XRD pattern of sample annealed at 973 K such that a new peak at 2θ = 95.577° can be observed which belongs to $Ni_4N(320)$ while $Ni_3N(111)$ peak is vanished. Hence, from the XRD results (Figure 1) of annealed samples it can clearly deduce that nickel nitride films are formed. Moreover, the increase of SS peaks intensity at 973 K relative to samples annealed at lower temperatures is due to the formation of deep and wide grooves in Ni film and detection of SS by XRD. The crystallite size, D, is obtained using the Scherrer equation (1) [20]:

$$D=\frac{k\lambda}{B\cos\theta} \qquad (1)$$

where, k is a dimensionless constant that is related to the shape and distribution of crystallites [21], λ is the wavelength of X-ray and θ is the Bragg angle. B is the full width at half maximum of the peak intensity (FWHM) bsed on equation (2):

$$B=\sqrt{W_0^2-W_i^2} \tag{2}$$

where, W_0 and W_i are the FWHM of the sample and of the stress-free sample (annealed powder sample), respectively.

The crystallite sizes resulted from the Scherrer relation and the full width at half maximum (FWHM) of the $Ni_3N(111)$ and $Ni_4N(320)$ peaks are given in column 3 of Table 1. It can be seen that with the increase of annealing temperature, the crystallite size of the nickel nitride phase is also increased.
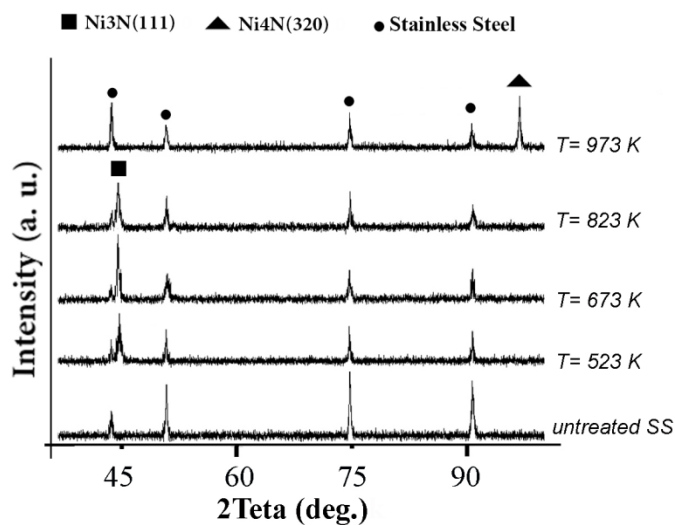
Figure 1: XRD Patterns of stainless steel and Ni/SS 304 samples annealed at different temperatures with flow of nitrogen.

Table 1: Crystallite size, surface roughness and passive current density of samples

Sample	T (K)	D_{XRD} (nm)	R_a (A°)	rms (A°)	Passive current density (µA cm^{-2})
1	Untreated SS	---	---	---	1218.12
2	523	11.02	41.04	46.65	97.85
3	673	14.43	46.12	49.97	24.71
4	823	36.93	64.31	69.07	972.23
5	973	37.25	76.94	82.09	579.60
T(K): annealing temperature, D_{XRD}: crystallite sizes obtained from XRD results, R_a: average surface roughness, rms: root mean square surface roughness					

3.2. AFM results

The AFM images of Ni/SS304 samples are given in Figure 2, while surface roughness of the samples obtained from the AFM measurements are given in Table 1. The results of AFM analysis of the samples show that when the annealing temperature is increased, the grains begin to grow. At the highest temperature, some grains show the effect of diffusion. In other words, due to the increase of diffusion process and mobility of smaller grains, they join to each other to form larger grains (Figure 2d). In addition, any increase in annealing temperature which causes the greater degrees of diffusion leads to rougher surfaces. Average and root mean square (rms) surface roughness results obtained from AFM measurements are observed in Table 1. It can be seen that surface roughness increases with temperature which, as discussed above,

can be the result of increased diffusion effect. In general, diffusion at higher temperatures is responsible for the grooving effect [22] which in turn increases the surface roughness due to the formation of deep grooves between very large grains that can even extend to the substrate surface (Figure 2d).

3.3. Polarization results

Potentiodynamic curves of samples annealed at different temperatures as well as the bare stainless steel are given in Figure 3. Table 1 also gives the electrochemical characteristics containing obtained from these curves. Electrochemical results show that the deposition of Ni on stainless steel substrates increases its resistance against acidic attack. The corrosion resistance of the samples decreases by increasing the annealing temperature above 673 K.
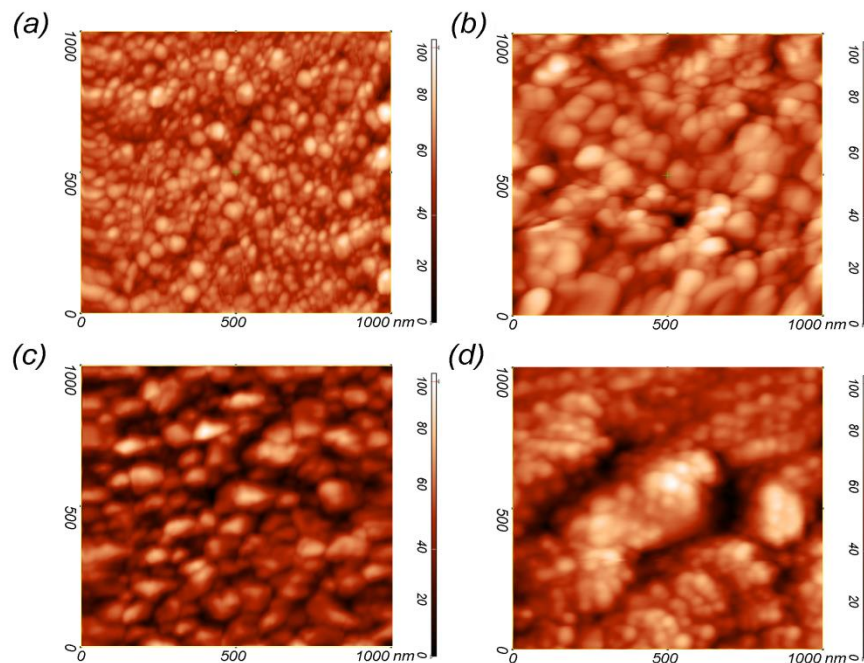
Figure 2: AFM images of; a-d) Ni/SS 304 samples annealed at different temperatures of 523, 673, 823 and 973 K, respectively
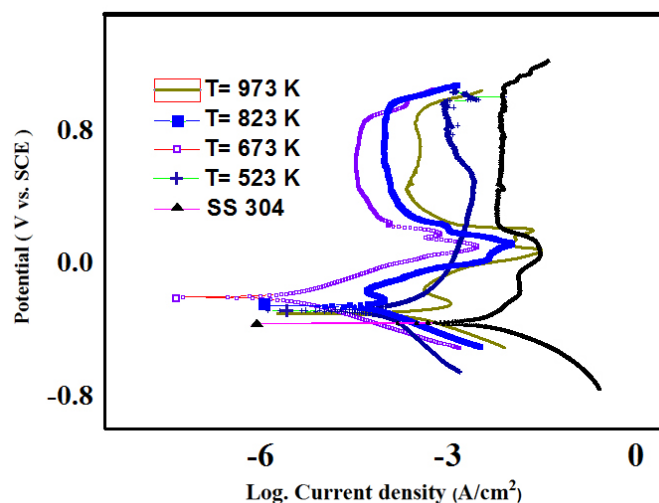
Figure 3: Potentiodynamic polarization curves for stainless steel and Ni/SS 304 samples annealed at different temperatures**.**
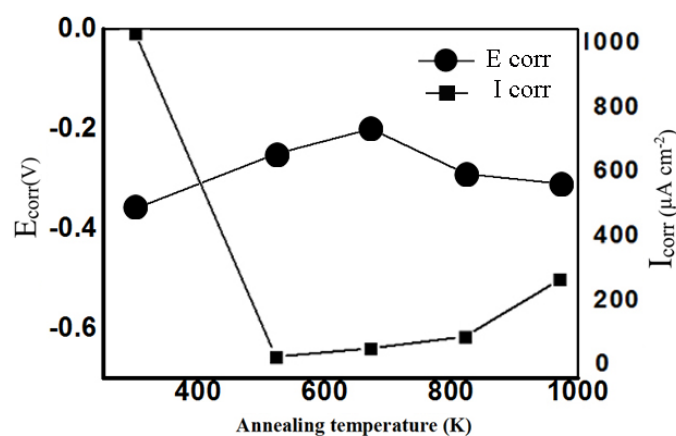
Figure 4: Ecorr and Icorr for stainless steel and Ni/SS 304 samples annealed at different temperatures.

The corrosion potential and corrosion current density versus annealing temperature are presented in Figure 4. For all the samples, corrosion potentials were higher than those for non-treated stainless steel. As shown in Figure 4, with the increase of annealing temperature to 523 K, corrosion potential increases while for the samples prepared above 673 K, some unexpectedly low values were obtained such that obtained value for the sample annealed at maximum annealing temperature is close to the value of the bare stainless steel. The presence of rough surface areas is responsible for the variation in the potential values

such that the obtained surface roughness from the AFM images in section 3.2 showed that the surface roughness increased with the annealing temperature due to the formation of larger grains and appearance of some grooves throughout the film. So, rough surface of samples prepared at high temperatures resulted in larger area being exposed to the corroding environment and it is also expected that the film become thinner in the grooves. Therefore, higher rate of corrosion reactions between these enlarged surface areas and the corroding solution is expected [22, 23]. The measured values of the corrosion current densities also clearly

confirm the effect of surface roughness on corrosion behavior of samples (Figure 4). All the annealed samples exhibit better corrosion resistance than the bare stainless steel. The corrosion current density is shifted to lower values in comparison to the bare stainless steel. The samples prepared at 673 K annealing temperature has the lowest corrosion current density. Furthermore, from the results of Table 1, it can also be observed that the lowest value of the passive current density belongs to the sample annealed at 673 K temperature.

3.4. SEM results

SEM micrographs in Figure 5 show the corroded surfaces of the samples examined after potentiodynamic polarization test. For the sample annealed at 523 K, only little damage on the surfaces was found and an example of it is presented in Figure 5a. For the sample prepared at 673 K, the corrosion behavior was different. Its surface was compact and seems not to have been affected by the corrosion test, i.e. its surface has the minimum effect of corroding media. For the higher treatment temperatures of 823 and 973 K, it could be seen that the corrosion attack was particularly strong so that the most corroded and damaged surface samples after corrosion test are the samples annealed at high temperatures of 823 and 973 K.

As discussed in section 3.2, AFM images of the samples showed that the samples annealed at 823 and 973 K have more rough surfaces. It can be concluded that the rough samples are susceptible to the corrosion attack since there are more ways for penetration of corroding media. Vice versa, there is minimum sign of corrosion attack for the samples with low annealing temperature which have smooth surfaces. The above presented discussion suggests that the protective behavior of the annealed samples is influenced by their morphology, roughness and porosity leading to defects such as pits and cracks.
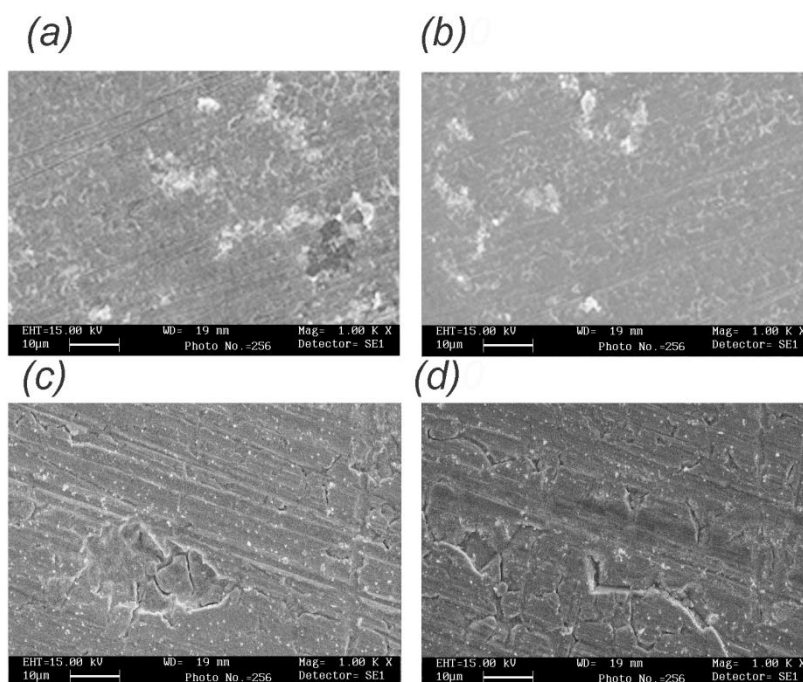
Figure 5: (a-d) SEM images of Ni/SS 304 samples annealed at different temperatures of 523, 673, 823 and 973 K, respectively.

4. Conclusions

The effect of annealing temperature under a nitrogen flow on corrosion behavior of nickel coated stainless steel was studied. Potentiodynamic polarization tests implemented to measure the corrosion resistance of the films were carried out in 1.0 M sulfuric acid solution. There is no direct relationship between the increase of annealing temperature and the protective properties of prepared samples. The film structures were analyzed using XRD and AFM before corrosion test and SEM after corrosion test. The films showed nickel nitride phases after annealing heat treatment process. Beside phase transition observed in XRD patterns, annealing process changed the surface properties. For temperatures higher than 673 K, heat treatment produced rough surfaces that have low corrosion resistance. In addition, the highest corrosion resistance among all prepared samples is achieved for the critical annealing temperature of 673 K. A good correlation was obtained between corrosion protection, structure and surface morphology.

5. References

1. R. Grayeli Korpi, Kh. M. Bahmanpour, Influence of Nitrogen Ion Implantation on the Structure and Corrosion Resistance of Stainless Steel Substrates Coated with Ni Nanolayer, *Prog. Color Colorants Coat*. 9(2016), 77-83

2. Mottu, M. Vayer, J. Dudognon, R. Erre, Structure and composition effects on pitting corrosion resistance of austenitic stainless steel after molybdenum ion implantation, *Surf. Coat. Technol.* 200(2005), 2131-2136.

3. P. Saravanan, V. S. Raja, S. Mukherjee, Effect of plasma immersion ion implantation of nitrogen on the wear and corrosion behavior of 316LVM stainless steel, *Surf. Coat. Technol.*, 201(2007), 8131 -8135.

4. V. B. Singh, The electrochemical behaviour of nitrogen-containing austenitic stainless steel in methanolic solution*, J Mater Sci.* 42(2007), 8279–8286

5. Y. Fu, X. Wu, E. Han, W. Ke, K. Yang, Z. Jiang, Effects of nitrogen on the passivation of nickel-free high nitrogen and manganese stainless steels in acidic chloride solutions, *Electrochim. Acta* 54(2009), 4005–4014.

6. T. CzerwiecU, N. Renevier 1, H. Michel, Low-temperature plasma-assisted nitriding, *Surf. Coat. Technol.* 131(2000), 267 -277

7. E. Menthe, K. Rie, Further investigation of the structure and properties of austenitic stainless steel after plasma nitriding, *Surf. Coat. Technol.*116–119 (1999), 199–204

8. M. Yatsuzuk, S. Miki, R. Morit, K. Azum, E. Fujiwar, H. Uchid, Enhanced corrosion resistance of TiN preparedby plasma-based ion implantation, *Vacuum* 59(2000), 330-337.

9. L. Nosei, S. Farina, M. Avalos, L. Nachez, B.J. Gomez, J. Feugeas, Corrosion behavior of ion nitrided AISI 316L stainless steel, *Thin Solid Films* 516(2008), 1044–1050.

10. Garcia, F. Martin, Y. Blanco, M. P. de Tiedra, M. L. Aparicio, Corrosion behaviour of duplex stainless steels sintered in nitrogen, *Corros. Sci*, 51(2009), 76-86.

11. A. R. Grayeli Korpi, Kh. M. Bahmanpour, Influence of nitrogen ion implantation on the structure and corrosion resistance of stainless steel substrates coated with Ni nanolayer, *Prog. Color Colorants Coat*. 9(2016), 77-83

12. Y.-Y. Chang, D.-Y. Wang, Corrosion behavior of electroless nickel-coated AISI 304 stainless steel enhanced by titanium ion implantation, *Surf. Coat. Technol.* 200 (2005), 2187–2191.

13. A. R. Grayeli-Korpi, H. Savaloni, Effect of nitrogen ion implantation on corrosion inhibition of nickel coated 316 stainless steel and correlation with nano-structure, *Appl. Surf. Sci.* 258 (2012), 9982–9988.

14. R. Winston Revie , Herbert H. Uhlig , corrosion and corrosion control, 4th Edition, JOHN WILEY & SONS, INC., PUBLICATION, 2008, 114-120

15. Liu, P. K. Chu, G. Lin, D. Yang, Effects of Ti/TiN multilayer on corrosion resistance of nickel–titanium orthodontic brackets in artificial saliva, *Corros. Sci.* 49 (2007), 3783–3796

16. Vempaire, S. Miraglia, A. Sulpice, L. Ortega, E.K. Hlil, D. Frucharta, J. Pelletier, Structure and magnetic properties of nickel nitride thin film synthesized by plasma-based ion implantation, *J. Magn. Magn. Mater.* 272–276 (2004), 843-844

17. V. Muthupandi, P. Bala Srinivasan, V. Shankar, S.K. Seshadri, S. Sundaresan, Effect of nickel and nitrogen addition on the microstructure and mechanical properties of power beam processed duplex stainless steel (UNS 31803) weld metals, *Mater. Lett.* 59 (2005), 2305 – 2309.

18. J. Baranowsk, B. Arnold, Corrosion resistance of nitrided layers on austenitic steel, *Surf. Coat. Technol.* 200 (2006) 6623–6628.

19. A. Abdel Aal, Development of nickel coatings by TiN interlayer, *Mater. Chem. Phys.* 106(2007), 317–322.

20. H. Klung, L. Alexander, X-Ray Diffraction Procedure, Wiley, New York, 1954, 503–524.

21. J. I. Langford, A. J. Wilson, Seherrer after sixty years: a survey and some new results in the determination of crystallite size, *J. Appl. Crystallogr.* 11 (1978), 102–113.

22. W. W. Mullins, The effect of thermal grooving on grain boundary motion, *Acta metal.*, 6 (1958), 414-427.

23. D.E. Aspnes, E. Kinsbron, D. D. Bacon, Optical properties of Au: Sample effects, Phys. Rev. B: Condens. *Matter Mater. Phys.*, 21(1980), 3290-3299.

How to cite this article:

A. R. Grayeli Korpi, Kh. M. Bahmanpour, Effect of Nitriding Temperature on the Nanostructure and Corrosion Properties of Nickel Coated 304 Stainless Steel. Prog. Color Colorants Coat., 10 (2017), 85-92.